Joint Spectrum/Beampattern Design of Wideband FM MIMO Radar Emissions

Patrick M. McCormick[1], Shannon D. Blunt[1] and Justin G. Metcalf[2]
[1]Radar Systems Lab, University of Kansas, Lawrence, KS
[2]Sensors Directorate, Air Force Research Laboratory, Dayton, OH

***Abstract*—The co-design of multiple-input multiple-output (MIMO) radar waveforms and the associated beampattern is desirable to maximize transmitted power in directions of interest while still maintaining acceptable waveform correlation properties. While MIMO is an emerging technology in radar, one must also consider the stringent spectral requirements that are currently being imposed now and that may become even more stringent in the future. In this paper a MIMO optimization method based on alternating projections is introduced that optimizes, for a uniform linear array, the constant-modulus, continuous-time, element-level waveforms to produce a spectral shape in various desired spatial directions denoted "beams of interest". The resulting beampattern is directly related to these chosen "beams of interest". To address the physical nature of the MIMO emission, the energy stored in the invisible space (i.e. not radiated into the far-field) is considered. It is shown that this stored energy, which could damage the transmitter if operated at high power, can effectively be minimized by optimizing the beampattern based on the visible emission space.**

Keywords—MIMO radar, beampattern design, waveform optimization

I. Introduction

The majority of multiple-input multiple-output (MIMO) beampattern/waveform design methods in the literature (for narrowband) approach waveform synthesis from a covariance matrix perspective given constraints such as constant amplitude (e.g. [1,2,3]). Wideband beamforming techniques have likewise been examined via optimization of the power allocation in space [4,5]. Wideband MIMO beampattern synthesis has also been studied in [6, 7]. In the spirit of [7], here a wideband MIMO emission optimization approach is developed that leverages recent work on the spectral shaping optimization of physically realizable FM waveforms [8,9], which is itself a specific manifestation of alternating projections [10,11,12]. In [8,9], the FM waveform power spectral density (PSD) was designed to possess a Gaussian shape, which corresponds to low autocorrelation sidelobes [13]. Here, this spectral shaping formulation is generalized for optimization of the emitted spectrum of a wideband MIMO emission transmitted from a uniform linear array (ULA). As such, the approach developed here represents a form of joint spectrum/beampattern design that provides the means to avoid damage that could otherwise occur due to the presence of reactive power caused by the MIMO emission.

For wideband MIMO emission optimization it is necessary to consider the possibility of storing energy in the reactive near-field of the array due to the electrical distance between adjacent elements being less than half-wavelength spacing for a significant portion of the bandwidth, which reduces the efficiency of the array and could damage the transmitter [14,15]. This storage of energy can also be viewed as emitting into the *invisible* (or non-radiating) space. Here it is shown that performing optimization that maximizes the power in the *visible* (radiating) emission space effectively serves to minimize the reactive power for frequencies corresponding to less than half-wavelength antenna spacing. Examples are shown in which the visible spectrum is optimized for both a widebeam MIMO emission (e.g. for synthetic aperture applications [16]) and multiple simultaneous narrow beams (e.g. for multi-mode operation [17]).

II. Wideband Array Analysis

Consider a uniform linear array (ULA) consisting of M elements with inter-element spacing d. A majority of the array analysis in literature is based on a narrowband model, which allows for the $M\times 1$ steering vector $\mathbf{v}(\theta)$ to be dependent on the center frequency f_{cent} as

$$\mathbf{v}(f_{\text{cent}},\theta)=\begin{bmatrix}1 & e^{j\frac{2\pi f_{\text{cent}}}{c}d\sin\theta} & \cdots & e^{j\frac{2\pi f_{\text{cent}}}{c}(M-1)d\sin\theta}\end{bmatrix}^T, \quad (1)$$

where c is the speed of light and θ is the spatial angle, with $\theta=0°$ defined as array boresight.

Let $s_m(t)$ be the pulsed waveform emitted from the mth antenna element, the discretized version of which is the $N\times 1$ vector $\mathbf{s}_m$ that is obtained by "over-sampling" $s_m(t)$ with respect to a selected bandwidth definition to ensure sufficient fidelity (Nyquist sampling cannot be achieved since this signal is not bandlimited). Collecting the M discretized waveforms into the $N\times M$ baseband waveform matrix $\mathbf{S}$, the discretized emission in spatial direction θ is $\mathbf{S}\mathbf{v}(f_{\text{cent}},\theta)$.

For a wideband emission from an array the relation of the bandwidth B to the maximum propagation time across the array $\Delta T_{\max}$ must be considered. If $(B\cdot\Delta T_{\max}<<1)$, the time delay can be treated as a phase shift. When this array narrowband assumption is violated, however, the signal at time t on one end of the array can differ significantly from the signal at time t on the other end of the array, thereby necessitating true time-delay processing to properly characterize the emission as a function of spatial angle.

The narrowband/wideband distinction also relates to the ratio of bandwidth to center frequency, otherwise known as *percent bandwidth*, which in principle could range from 0% to 200%. A percent bandwidth at or below 10% is generally considered narrowband. For higher percent bandwidth, consideration of antenna element spacing as a function of frequency is necessary as this relationship directly impacts the

This work was supported by a subcontract with Matrix Research, Inc. for research sponsored by AFRL under Prime Contract # FA8650-14-D-1722.

amount of reactive power versus radiated power, particularly for widebeam MIMO emissions.

A. *Wideband Beamforming*

The frequency content of each of the M waveforms at passband frequency f can be found by performing

$$\mathbf{s}(f) = \mathbf{a}^H(f)\mathbf{S}, \tag{2}$$

where

$$\mathbf{a}(f) = \left[1 \quad e^{j2\pi(f-f_{\text{cent}})/f_{\text{samp}}} \quad \cdots \quad e^{j2\pi(N-1)(f-f_{\text{cent}})/f_{\text{samp}}}\right]^T \tag{3}$$

is an $N\times 1$ vector with f_{samp} the sampling frequency, and $\mathbf{s}(f)$ is $1\times M$. Noting that (1) can be generalized for arbitrary frequency f as $\mathbf{v}(f,\theta)$, the frequency content of the MIMO emission in direction θ can be determined as

$$g(f,\theta) = \mathbf{a}^H(f)\mathbf{S}\,\mathbf{v}(f,\theta), \tag{4}$$

which shall be used for joint spectrum/beamforming design. It is also useful to define the electrical phase angle

$$\phi(f,\theta) = \frac{2\pi f}{c} d\sin\theta, \tag{5}$$

which, for a ULA, represents the phase difference between adjacent antenna elements for a given spatial angle θ as a function of frequency f.

This narrowband component of the wideband emission corresponds to a true-time delay for the mth element versus θ of

$$\Delta\tau_m = m\frac{d}{c}\sin\theta \tag{6}$$

for $m = 0,1,\ldots,M-1$. The maximum delay across the array is thus $\Delta\tau_{\max} = (M-1)d/c$. Since the optimization is performed in the discrete-time/frequency domains care must be taken such that the time-shifted signals do not alias. Zero-padding in the time domain (or oversampling in the frequency domain) allows room for the signals to shift. The amount of padding necessary is dictated by the maximum sample shift $\lceil f_{\text{samp}}\Delta T_{\max}\rceil$, where $\lceil\bullet\rceil$ is the ceiling operation.

B. *Percent Bandwidth*

The percent bandwidth of an emission is defined as

$$\%BW = \frac{B}{f_{\text{cent}}}. \tag{7}$$

For high percent bandwidth the beam pattern is distorted over the band due to the array looking electrically small in lower frequencies and electrically large in higher frequencies.

For non-bandlimited signals it is important to consider the definition of bandwidth B, examples of which include 3-dB, 10-dB, 95% power, and 98% power. Defining the bandwidth in terms of percent power allows for an easy comparison between different spectral shapes. Thus 98% power bandwidth shall be used here.

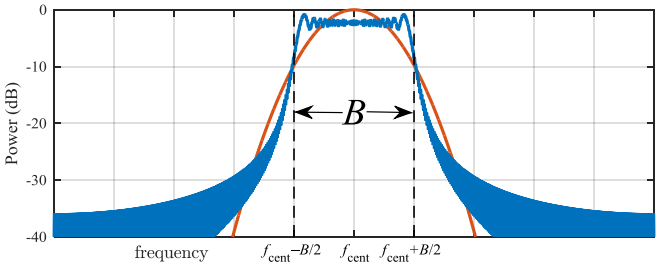

Fig. 1. 98% power bandwidth B for Gaussian spectral shape (red) and linear frequency modulated waveform (blue)

Figure 1 shows the 98% bandwidth for a linear frequency modulated (LFM) waveform and a Gaussian-shaped spectrum. Notice that the bandwidth for these spectra (normalized to have equal energy) corresponds to different power levels (about –6 dB from the peak for LFM and about –10 dB from the peak for the Gaussian spectrum), yet the same amount of power is contained inside B.

C. *Reactive vs. Radiated Power*

An array with element spacing less than $\lambda_{\text{cent}}/2$, where λ_{cent} is the wavelength corresponding to center frequency f_{cent}, can emit power into what is known as the *invisible* space [14]. The invisible space is electrically located beyond the electrical angle of the endfire directions (at $\theta = \pm\pi/2$ or $\phi = \pm\pi$). In this case, a widebeam MIMO radiation pattern with a near-omnidirectional beampattern can have a significant fraction of the total power emitted into this invisible space. The word "emitted" is really a misnomer in this context because the power is not actually transmitted into the environment but results in energy stored in the reactive near field of the array, which can lead to a large amount of reflected power that may damage the transmitter [14].

For narrowband emissions the energy stored from radiating into the invisible space is avoided by defining the array with $d = \lambda_{\text{cent}}/2$ spacing. For wideband emissions, however, a significant range of wavelengths inside the bandwidth correspond to an inter-element electrical spacing that is less than $\lambda/2$.

To illustrate the issue of reactive power for a wideband emission, consider how one could produce a MIMO emission that is omnidirectional (in terms of average power). Given 30 elements in a ULA with $\lambda_{\text{cent}}/2$ spacing, it is possible to design the emission to possess a Gaussian spectral shape for all electrical angles in (5) (or all spatial angles for a narrowband case).

Figure 2 shows the frequency content of the emission (normalized by f_{cent}) versus the sine of the spatial angle θ. However, the reactive power is not shown in this image. In contrast, Fig. 3 shows the same spectrum in terms of electrical angle from (5). The vertical dashed lines indicate where $\phi = \pm\pi$ occur, which define the endfire directions for a half-wavelength, narrowband array. The solid black, diagonal lines demarcate the bounds for the *visible* (or radiated) space. The

slope of this bound is directly related to %BW from (7). Under the narrowband assumption, this line is vertical. The frequency point at which the dashed and solid lines intersect is the frequency for which the half-wavelength element spacing is based (here f_{cent}, and thus $\lambda_{\text{cent}}/2$). The red triangles in Fig. 3 identify the regions in which energy would be stored in the near field. Even when the amount of this stored energy is not sufficient to damage the transmitter via reflected power, from an efficiency perspective it is less than optimal.

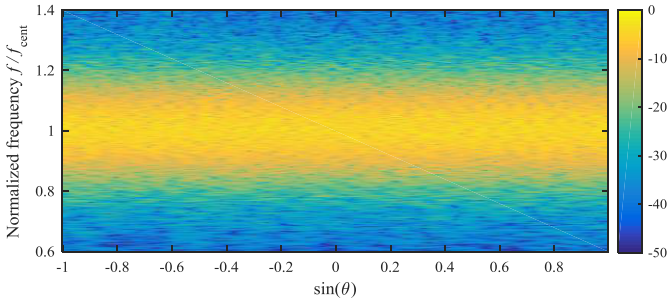

Fig. 2. Wideband frequency content vs. sin(θ) for omnidirectional MIMO emission with $d = \lambda_{\text{cent}}/2$ and 30% bandwidth.

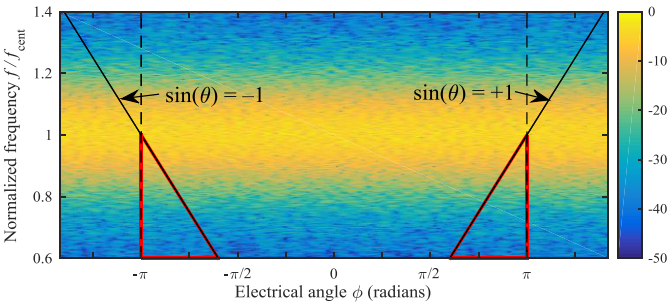

Fig. 3. Wideband frequency content vs. electrical angle $\phi(f,\theta)$ for omnidirectional MIMO emission with $d = \lambda_{\text{cent}}/2$ and 30% bandwidth. The red triangles identify the reactive power region.

There are three ways to reduce the amount of power stored in the invisible space: *a*) increase the spacing between elements, thereby lowering the intersection point of the dashed and dotted line in Fig. 3; *b*) constraining the phase difference between adjacent elements; or *c*) through optimization of the spectral content emitted into the visible/invisible spaces. The first method involves setting element spacing based on the lowest frequency in the band, which conflicts with typical designs that set this spacing according to the highest frequency to avoid grating lobes [18]. The second method is a waveform-centric perspective that, while valid, is an indirect way in which to address the actual problem. In contrast, the final approach of shaping the visible/invisible spectrum directly addresses the problem by maximizing the power in the visible space (and thereby effectively minimizing the power in the invisible space).

Mutual coupling effects are also known to distort MIMO emissions [19,20]. Therefore care must be taken when antenna elements are electrically close (less than half-wavelength spacing), which tends to increase coupling between elements. While such effects are not addressed here, a frequency-dependent mutual coupling model could readily be implemented into the joint spectrum/beampattern optimization process.

III. MIMO Joint Spectrum/Beampattern Optimization

The proposed algorithm is a generalization of the spectrum shaping approach developed in [8] that realized a non-repeating FM continuous wave (FMCW) waveform, the performance of which was demonstrated experimentally. A similar version of the approach was used to optimize jointly an FM waveform and low-loss (0.26 dB) amplitude taper that was experimentally demonstrated in [9] to achieve range sidelobes better than −83 dB. The design approach of [8,9] alternates between shaping the PSD of a waveform to achieve a desired spectral window (including both in-band and roll-off spectrum) and shaping the time-domain structure (to be either constant amplitude or low-loss), until convergence is reached. This approach is a specific form of alternating projection optimization [10,11,12].

Here the waveform design approach of [8,9] is generalized to shape the spectrum over a set of spatial angles denoted as the "beams of interest" of a wideband MIMO emission. The resulting set of M MIMO signals are FM waveforms, and thus are constant amplitude, possess good spectral containment, and are amenable to a high-power transmitter. Further, the joint spectrum/beampattern optimization ensures that minimal power is emitted into the invisible space. While the optimization involves determining the discrete samples in $\mathbf{S}$, the combination of 1) being oversampled relative to a selected bandwidth definition, 2) accounting for realistic spectral roll-off, and 3) constraining to constant amplitude, ensures sufficient fidelity to closely approximate FM waveforms that can readily be implemented via [21] onto an arbitrary waveform generator.

A. *Initialization of optimization parameters*

Consider a ULA containing M elements of spacing d (though other array configurations are also possible). Denote θ_p, for $p = 0,1,\ldots,P-1$, as the spatial angles of the P "beams of interest" to be included in the optimization. Likewise, define Q distinct equally-spaced frequencies

$$f_q = \frac{-f_{\text{samp}}}{2} + \frac{q}{Q} f_{\text{samp}}, \tag{8}$$

for $q = 0,1,\ldots,Q-1$, such that the discretized passband frequency f is

$$f = f_q + f_{\text{cent}}, \tag{9}$$

with the requirement that $Q \geq N + \left\lceil f_{\text{samp}} \Delta T_{\max} \right\rceil$ for N the discretized length of the "oversampled" waveforms (relative to a selected bandwidth definition).

Inserting (8) and (9) into (3) yields

$$\mathbf{a}(f_q) = \left[1 \quad e^{j2\pi(-1/2+q/Q)} \quad \cdots \quad e^{j2\pi(N-1)(-1/2+q/Q)}\right]^T \tag{10}$$

for $q = 0,1,\ldots,Q-1$.

It is convenient to define the half-wavelength element spacing d with respect to the wavelength λ_d, and associated frequency f_d upon which it is based, as

$$d = 0.5\lambda_d = 0.5\frac{c}{f_d}. \tag{11}$$

Then inserting (8), (9) and (11) into (5) and enforcing the dependence on f_q and θ_p yields the discretization of electrical phase angle as

$$\phi(f_q,\theta_p) = \pi\frac{\left(f_{\text{samp}}\left(-\frac{1}{2}+\frac{q}{Q}\right)+f_{\text{cent}}\right)}{f_d}\sin\theta_p \tag{12}$$

for $q = 0,1,\ldots,Q-1$ and $p = 0,1,\ldots,P-1$. Here the sampling frequency f_{samp} is chosen to be K times the 98% bandwidth B (so $f_{\text{samp}} = KB$) to provide enough "over-sampling" to ensure sufficient waveform fidelity (minimal aliasing). Inserting this relationship into (11) and dividing the numerator and denominator by the center frequency f_{cent} yields

$$\phi(f_q,\theta_p) = \pi\frac{\left(\%BW\times K\left(-\frac{1}{2}+\frac{q}{Q}\right)+1\right)}{f_d / f_{\text{cent}}}\sin\theta_p, \tag{13}$$

which can readily be inserting into (1) to form the steering vectors $\mathbf{v}(f_q,\theta_p)$. The formulation in (13) allows for direct implementation of a desired %BW. The ratio f_d / f_{cent} sets the intersection point of $\sin\theta = \pm 1$ and $\phi = \pm\pi$ as described in Fig. 3, which subsequently dictates the antenna spacing.

Note that the "oversampling" factor K must also be taken into account when forming the spectral window. For an oversampling of K, the 98% bandwidth should be contained in $1/K$th of the total spectral window centered at f_{cent}. Also, for time-bandwidth product BT and "over-sampling" factor K, the length of each discretized waveform is $N = K(BT)$.

B. Spectral shaping via alternating projections

The spectral content for frequency f_q and spatial angle θ_p can be expressed as

$$g(f_q,\theta_p) = \mathbf{a}^H(f_q)\mathbf{S}\,\mathbf{v}(f_q,\theta_p) \tag{14}$$

for initial $N\times M$ waveform matrix $\mathbf{S}$.

Define $\mathbf{V}(f_q) = [\mathbf{v}(f_q,\theta_0)\ \ \mathbf{v}(f_q,\theta_1)\ \ \cdots\ \ \mathbf{v}(f_q,\theta_{P-1})]$ as the $M\times P$ steering vector matrix for frequency f_q. Thus the spectral content at frequency f_q across the P spatial angles can be written as the $1\times P$ vector

$$\mathbf{g}(f_q) = \mathbf{a}^H(f_q)\mathbf{S}\,\mathbf{V}(f_q). \tag{15}$$

Stacking the Q instantiations of (14) associated with baseband frequencies f_q for $q = 0,1,\ldots,Q-1$ yields the $Q\times P$ discretized spectrum matrix $\mathbf{G}$ for frequencies f_0 through f_{Q-1} and angles θ_0 through θ_{P-1} as

$$\mathbf{G} = \begin{bmatrix} g(f_0,\theta_0) & g(f_0,\theta_1) & \cdots & g(f_0,\theta_{P-1}) \\ g(f_1,\theta_0) & g(f_1,\theta_1) & \cdots & g(f_1,\theta_{P-1}) \\ \vdots & \vdots & \ddots & \vdots \\ g(f_{Q-1},\theta_0) & g(f_{Q-1},\theta_1) & \cdots & g(f_{Q-1},\theta_{P-1}) \end{bmatrix}. \tag{16}$$

Now define the $Q\times P$ spectral shaping matrix as

$$\mathbf{U} = \left[b(\theta_0)\mathbf{u}(\theta_0)\ \ b(\theta_1)\mathbf{u}(\theta_1)\ \ \cdots\ \ b(\theta_{P-1})\mathbf{u}(\theta_{P-1})\right], \tag{17}$$

where $\mathbf{u}(\theta_p)$ is the length-Q spectral shaping template (e.g. Gaussian) associated with the pth beam of interest and $b(\theta_p)$ is an adaptive scaling that dictates the relative contributions of the P beams so as to achieve the desired joint spectrum/beampattern. The ith iteration of $b(\theta_p)$ is defined as

$$b_i(\theta_p) = b_{i-1}(\theta_p)\sqrt{\frac{\mathbf{u}^H(\theta_p)\mathbf{u}(\theta_p)}{\sum_{q=0}^{Q-1}\left|g_i(f_q,\theta_p)\right|^2\sum_{\ell=0}^{P-1}\left|b_{i-1}(\theta_\ell)\right|^2}}. \tag{18}$$

Spectral shaping is thus performed as

$$\tilde{\mathbf{G}}_{p,q} = \mathbf{U}_{p,q}\exp\left(j\angle\mathbf{G}_{p,q}\right) \tag{19}$$

for $p = 0,1,\ldots,P-1$ and $q = 0,1,\ldots,Q-1$.

Next define $\tilde{\mathbf{r}}(f_q)$ as the $1\times M$ vector associated with frequency f_q that has been projected back onto the array via

$$\tilde{\mathbf{r}}(f_q) = \tilde{\mathbf{g}}(f_q)\mathbf{V}^H(f_q), \tag{20}$$

where $\tilde{\mathbf{g}}(f_q)$ is the qth row of $\tilde{\mathbf{G}}$. Stacking the Q frequency-dependent $1\times M$ vectors from (20) and pre-multiplying by the collection of $N\times 1$ vectors from (10) for the Q frequencies yields the $N\times M$ matrix

$$\tilde{\mathbf{S}} = \left[\mathbf{a}(f_0)\ \ \mathbf{a}(f_1)\ \ \cdots\ \ \mathbf{a}(f_{Q-1})\right]\begin{bmatrix}\tilde{\mathbf{r}}(f_0)\\ \tilde{\mathbf{r}}(f_1)\\ \vdots \\ \tilde{\mathbf{r}}(f_{Q-1})\end{bmatrix}. \tag{21}$$

The final step is to apply the constant amplitude constraint by simply extracting the phase as

$$\mathbf{S}_{n,m} = \exp(j\angle\tilde{\mathbf{S}}_{n,m}), \tag{22}$$

for $n = 0,1,\ldots,N-1$ and $M = 0,1,\ldots,M-1$, which contains M "over-sampled" discretized FM waveforms that could be loaded onto arbitrary waveform generators (AWGs) for emission from a MIMO radar (noting that additional up-sampling is likely necessary for AWG implementation).

The process of (15) – (22) is repeated until convergence. Table I provides an overview of the design procedure. Note

that this optimization method does not explicitly minimize the correlation between the M element-level waveforms. However, it should be noted that the solution obtained is certainly dependent on the initialization of the waveform matrix $\mathbf{S}$. For example, if this waveform matrix is initialized with random signals, the resulting set of optimized FM waveforms will retain some of the uncorrelated properties of such an initialization.

TABLE I
IMPLEMENTATION OF WIDEBAND MIMO SPECTRUM/BEAMPATTERN SHAPING

1.	Establish the number of antenna elements M and discretized waveform length N for "oversampling" K and time-bandwidth product BT.
2.	Select quantity P and specific directions θ_p of the beams of interest, the number of frequency bins Q, percent bandwidth $\%BW$, and the ratio f_d/f_{cent} that dictates element spacing.
3.	Form the spectral shaping vector $\mathbf{u}(\theta_p)$ for each of the P beams of interest.
4.	Initialize waveform matrix $\mathbf{S}^{(0)}$, loop index $i=1$, and scaling coefficients $b_0(\theta_p)$ to unity.
5.	Form $\mathbf{G}^{(i)}$ for frequencies f_q and angles θ_p using (1), (10), (13), (15) and (16), update scaling coefficients $b_i(\theta_p),\ldots,b_i(\theta_{P-1})$ via (18).
6.	Apply spectral shaping $\mathbf{U}$ via (19) to form $\tilde{\mathbf{G}}^{(i)}$.
7.	Form the unconstrained waveform matrix $\tilde{\mathbf{S}}^{(i)}$ via (20) and (21).
8.	Apply constant amplitude constraint to waveform matrix via (22) to form updated waveform matrix $\mathbf{S}^{(i)}$.
9.	Stop if adequately converged. Otherwise, increment $i=i+1$ and go to step 5.

IV. OPTIMIZATION EXAMPLES

Consider a waveform matrix optimized for a time-bandwidth of 100 and oversampling $K=5$, such that $N=5(100)=500$ with percent bandwidth $\%BW=30\%$. The array is a ULA consisting of 30 elements with element spacing d, which is set according to the highest frequency within the 98% bandwidth B. The normalized frequency associated with this spacing is

$$\frac{f_d}{f_{\text{cent}}}=\frac{f_{\text{cent}}+B/2}{f_{\text{cent}}}=1+\frac{\%BW}{2}=1.15. \tag{23}$$

The maximum sample delay for this array is

$$f_{\text{samp}}\cdot\Delta\tau_{\max}=KB\cdot\frac{(M-1)d}{c}=(M-1)\frac{K\times\%BW}{2\,f_d/f_{\text{cent}}}\simeq 18.915. \tag{24}$$

Therefore a minimum of 19 samples are needed to account for the maximum sample shift of $Q\geq N+\left\lceil f_{\text{samp}}\Delta\tau_{\max}\right\rceil=500+19$. The number of frequency points is chosen to be $Q=2N=1000$, which is much greater than the minimum samples of 519.

We wish to realize an omnidirectional beampattern (such as in Fig. 3), albeit with minimal emission into the invisible space. The number of beams of interest is set to $P=2M=60$, such that

$$\theta_p=\sin^{-1}\left(-1+2\frac{(p+0.5)}{P}\right) \tag{25}$$

for $p=0,1,\ldots,P-1$. Note that these beams are equally spaced in $\sin\theta$ space and exclude the extreme cases of $\sin\theta=\pm1$ so as to account for non-infinitesimal width of the beams.

Gaussian spectrum shaping (Fig.1) is used for all of the 60 beams of interest. The waveform matrix $\mathbf{S}^{(0)}$ is initialized using complex white Gaussian noise of unit variance and zero mean to realize a final set of FM waveforms that are relatively uncorrelated.

Figure 4 shows the wideband spectrum of the isotropic MIMO emission with 30% bandwidth versus electrical angle ϕ after 500 iterations of the design procedure. Notice that there is little power radiated into the invisible space as compared to the unconstrained MIMO emission from Fig. 3. Figure 5 shows the MIMO beampattern for this near-omnidirectional emission. Due to the scaling coefficients from (17) and (18), the beampattern is relatively flat in the angular region of interest, with less than 0.5 dB variation. Figure 6 shows the maximal spectral powers across all θ, overlaid with the desired spectrum shape. Notice that the tails of the emission spectrum (blue) deviate from the spectral mask (red), which is due to the constant amplitude constraint preventing a perfect fit to the mask.

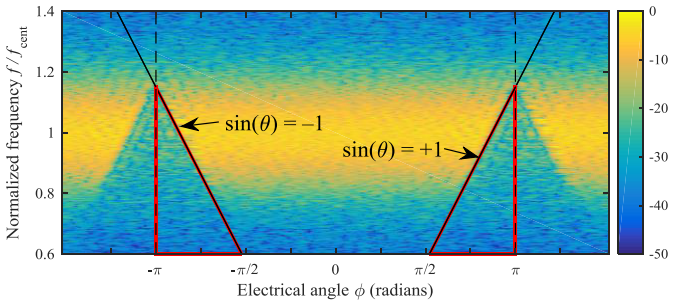

Fig. 4. Spectrum of omnidirectional wideband (30% BW) MIMO emission versus electrical angle ϕ

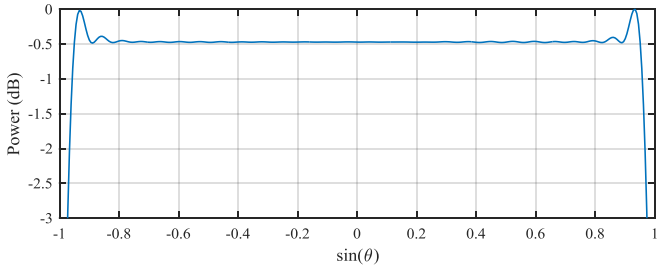

Fig.5. Peak-normalized near-omnidirectional MIMO beampattern versus $\sin\theta$

In contrast to the omnidirectional beampattern, now consider the case when only $P=4$ beams are desired in directions $\theta=[-40^\circ\ \ -10^\circ\ \ 0^\circ\ \ 20^\circ]$, thus resulting in a wideband multi-beam MIMO emission. The relative powers of the spectra are set such that $\theta=-40^\circ$ is 6 dB larger in power

compared to the other three beams. The other parameters remain the same as the last example.

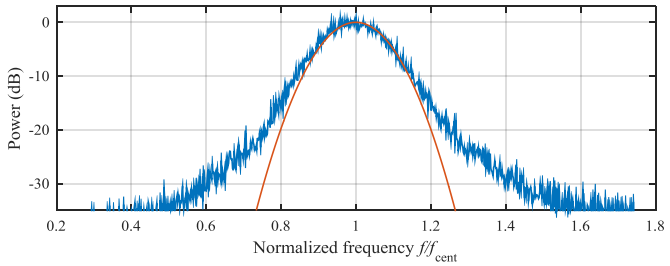

Fig. 6. Maximum spectral powers over all space θ for each normalized frequency (blue) and spectral window used in optimization (red)

Figure 7 shows the wideband spectrum for this emission scheme. All four beams are clearly visible and well-approximate the Gaussian spectral shape. Notice again that there is minimal power radiated into the invisible region. Figure 8 shows the peak-normalized MIMO beampattern for this wideband emission. The angles/powers of the beams match exactly to the desired emission structure, with the beam at angle $\theta = -40°$ being 6 dB greater than the others.

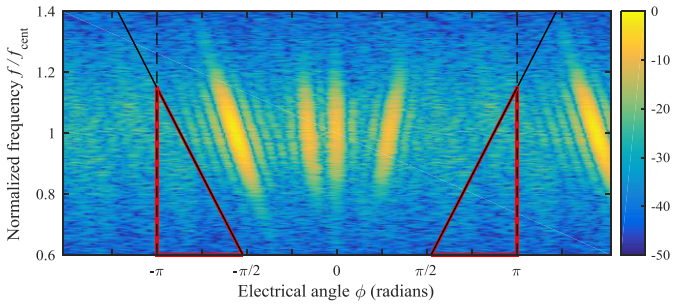

Fig. 7. Spectrum of wideband (30% bandwidth) multi-beam MIMO emission versus electrical angle ϕ

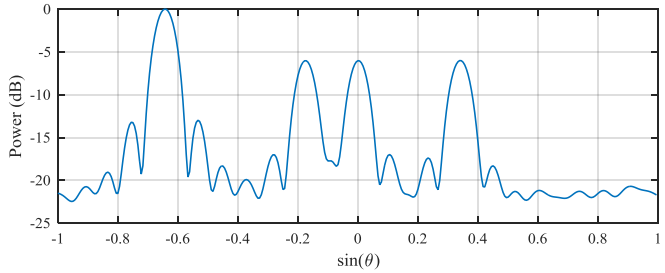

Fig. 8. Peak-normalized multi-beam-MIMO beampattern versus $\sin\theta$

V. Conclusion

A wideband MIMO optimization approach has been developed that shapes the spectrum of spatial "beams of interest" while effectively minimizing the power that would otherwise be wasted in the invisible space (and which could damage the transmitter). The resulting MIMO waveforms have constant amplitude and closely approximate FM, such that they can be readily implemented on a high power system. The flexibility of the emission design approach was demonstrated via simulation by generating a near-omnidirectional MIMO emission and a multi-beam MIMO emission.

References

[1] D.R. Fuhrmann and G.S. Antonio "Transmit beamforming for MIMO radar systems using signal cross-correlation", *IEEE Trans. Aerosp. Electron. Syst.*, vol. 44, no. 1, pp.1 -16, Jan. 2008.

[2] S. Ahmed, J.S. Thompson and B. Mulgrew, "Unconstrained synthesis of covariance matrix for MIMO radar transmit beampattern," IEEE *Trans. Signal Processing*, vol. 59, no. 8, pp. 3837 - 3849, Aug. 2011.

[3] P. Stoica , J. Li and X. Zhu "Waveform synthesis for diversity-based transmit beampattern design", *IEEE Trans. Signal Process.*, vol. 56, no. 6, pp.2593 -2598, June 2008.

[4] D.P. Scholnik and J.O. Coleman "Optimal design of wideband array patterns", *IEEE Intl. Radar Conf*, Washington, DC, May 2000.

[5] D.P. Scholnik and J.O. Coleman "Optimal array-pattern synthesis for wideband digital transmit arrays", *IEEE J. Sel. Topics in Signal Process.*, vol. 1, no. 4, pp.660 -677, Dec. 2007.

[6] G.S. Antonio, D.R. Fuhrmann, "Beampattern synthesis for wideband MIMO radar systems". *IEEE Computational Advances in Multi-Sensor Adaptive Processing*, Puerto Vallarta, Mexico, pp. 105-108, Dec. 2005.

[7] H. He, P. Stoica, and J. Li, "Wideband MIMO systems: signal design for transmit beampattern synthesis," *IEEE Trans. Signal Process*., vol. 59, pp. 618-628, Feb. 2011.

[8] J. Jakabosky, S.D. Blunt, and B. Himed, "Waveform design and receive processing for nonrecurrent nonlinear FMCW radar" *IEEE Intl. Radar Conf.*, Washington, DC, May 2015.

[9] J. Jakabosky, S.D. Blunt, and T. Higgins, "Ultra-low sidelobe waveform design via spectral shaping and LINC transmit architecture" *IEEE Intl. Radar Conf.*, Washington, DC, May 2015.

[10] H.H. Bauschke and J.M. Borwein, "On projection algorithms for solving convex feasibility problems," *SIAM Review*, vol. 38, no. 3, pp. 367-426, Sept. 1996.

[11] A. Levi and H. Stark, "Image restoration by the method of generalized projections with application to restoration from magnitude," *J. Opt. Soc. Am.*, vol. 1, no. 9, pp. 932-943, Sept. 1984.

[12] O.M. Bucci, G. Franceschetti, G. Mazzarella, and G. Panariello, "Intersection approach to array pattern synthesis," *IEE Proc. H – Microwaves, Antennas and Propagation*, vol. 137, no. 6, pp. 349-357, Dec. 1990.

[13] J.A. Johnston and A.C. Fairhead, "Waveform design and Doppler sensitivity analysis for nonlinear FM chirp pulses," *IEE Proc. F – Communications, Radar & Signal Processing*, vol. 133, no. 2, pp. 163-175, Apr. 1986.

[14] G. Frazer, Y. Abramovich, and B. Johnson, "Spatially waveform diverse radar: perspectives for high frequency OTHR," *IEEE Radar Conf.*, pp. 385–390, Boston, MA, USA, 2007.

[15] F. Daum and J. Huang, "MIMO radar: snake oil or good idea?" *IEEE Aerospace & Electronic Systems Mag.*, vol. 24, no. 5, pp. 8-12, May 2009.

[16] G. Krieger, "MIMO-SAR: opportunities and pitfalls," *IEEE Trans. Geoscience & Remote Sensing*, vol. 52, no. 5, pp. 2628-2645, May 2014.

[17] G.C. Tavik, et al, "The advanced multifunction RF concept," *IEEE Trans. Microwave Theory & Techniques*, vol. 53, no. 3, pp. 1009-1020, Mar. 2005.

[18] J.D. Taylor, ed. *Introduction to ultra-wideband radar systems*. CRC press, 1994.

[19] B. Cordill, J. Metcalf, S.A. Seguin, D. Chatterjee, and S.D. Blunt, "The impact of mutual coupling on MIMO radar emissions," *IEEE Intl. Conf. EM in Advanced Applications*, Turino, Italy, pp. 644-647, Sept. 2011.

[20] G. Babur, P.J. Aubry, and F. Le Chevalier, "Antenna coupling effects for space-time radar waveforms: analysis and calibration," *IEEE Trans. Antennas & Propagation*, vol. 62, no. 5, pp. 2572–2586, May 2014.

[21] S.D. Blunt, J. Jakabosky, M. Cook, J. Stiles, S. Seguin, and E.L. Mokole, "Polyphase-coded FM (PCFM) radar waveforms, part II: optimization," *IEEE Trans. Aerospace & Electronic Systems*, vol. 50, no. 3, pp. 2230-2241, July 2014.